Supplementary information

Reduced Co_3O_4 Nanowires with Abundant Oxygen Vacancies as Efficient Free-standing Cathode for Li-O_2 Batteries

Fang Wang, Wang Liu, Hui Wang,Chengcheng Meng, Qixing Wu, Xuelong Zhou, Zhongkuan Luo*

College of Chemistry and Environmental Engineering, Shenzhen University, Shenzhen 518060, Guangdong, China

*Corresponding author. Tel: 0755-26557381; Fax: 0755-26536141

E-mail addresses: lzk@szu.edu.cn (Z. Luo).

Co_3O_4 nanoarrays grown directly on Ni foam substrate was obtained by facile hydrothermal and calcination process. With the increase of NH_4F content, the loading mass density of nanoarrays became higher, leading to three types of morphology, which were nanowires, nanonorods and nanosheets, respectively (Fig. S1).

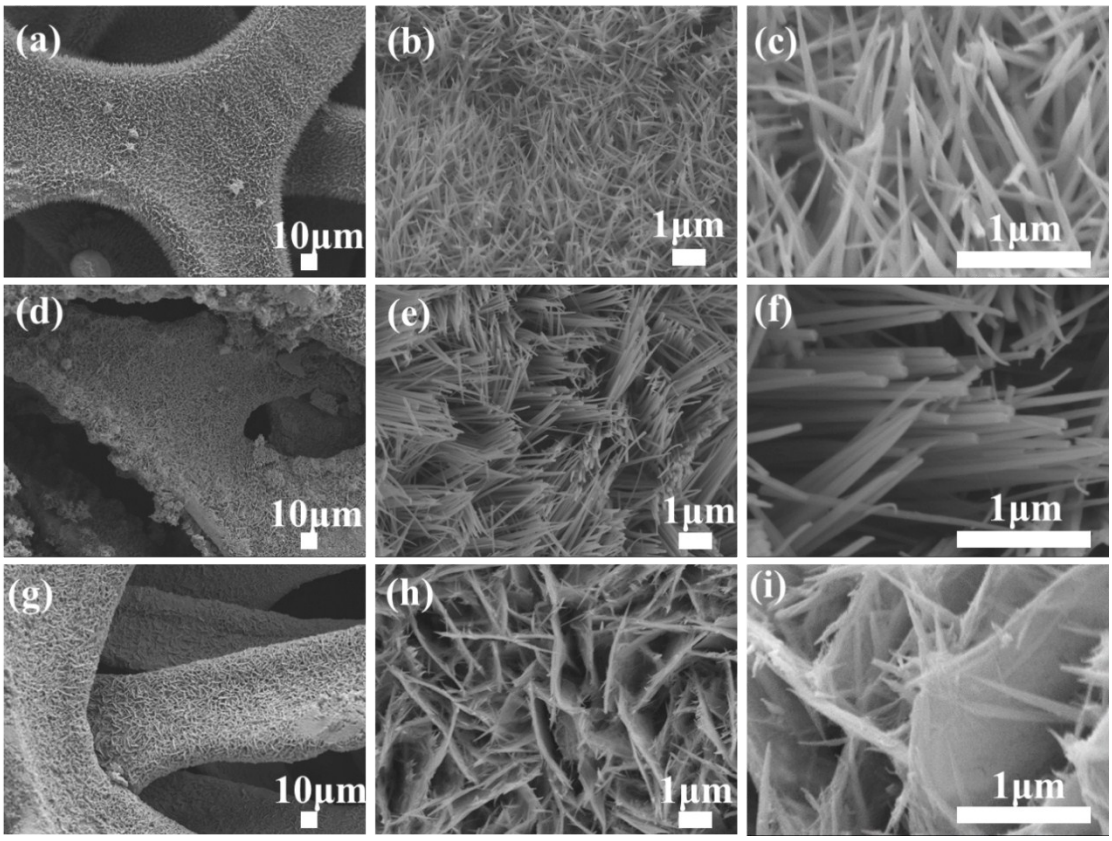

Fig. S1 SEM images of (a, b, c) Co_3O_4 nanowires, (d, e, f) Co_3O_4 nanorods, (g, h, i) Co_3O_4 nanosheets.

The three samples were analyzed by transmission electron microscopy (Fig. S2). It can be seen that the nanoarrays surface was rough, consisting of many small nanoparticles with copious mesopores. As shown in the select area electron diffraction, nanowires and nanosheets show polycrystalline characteristics, nanorods displayed a quasi-single crystal structure. The high–resolution TEM images in Fig. S2b, d, f

reveal three types of lattice fringes with interplane spacings of 0.46, 0.28 and 0.23nm, respectively, corresponding to the (111), (220) and (222) planes of the cubic spinel Co_3O_4 phase.

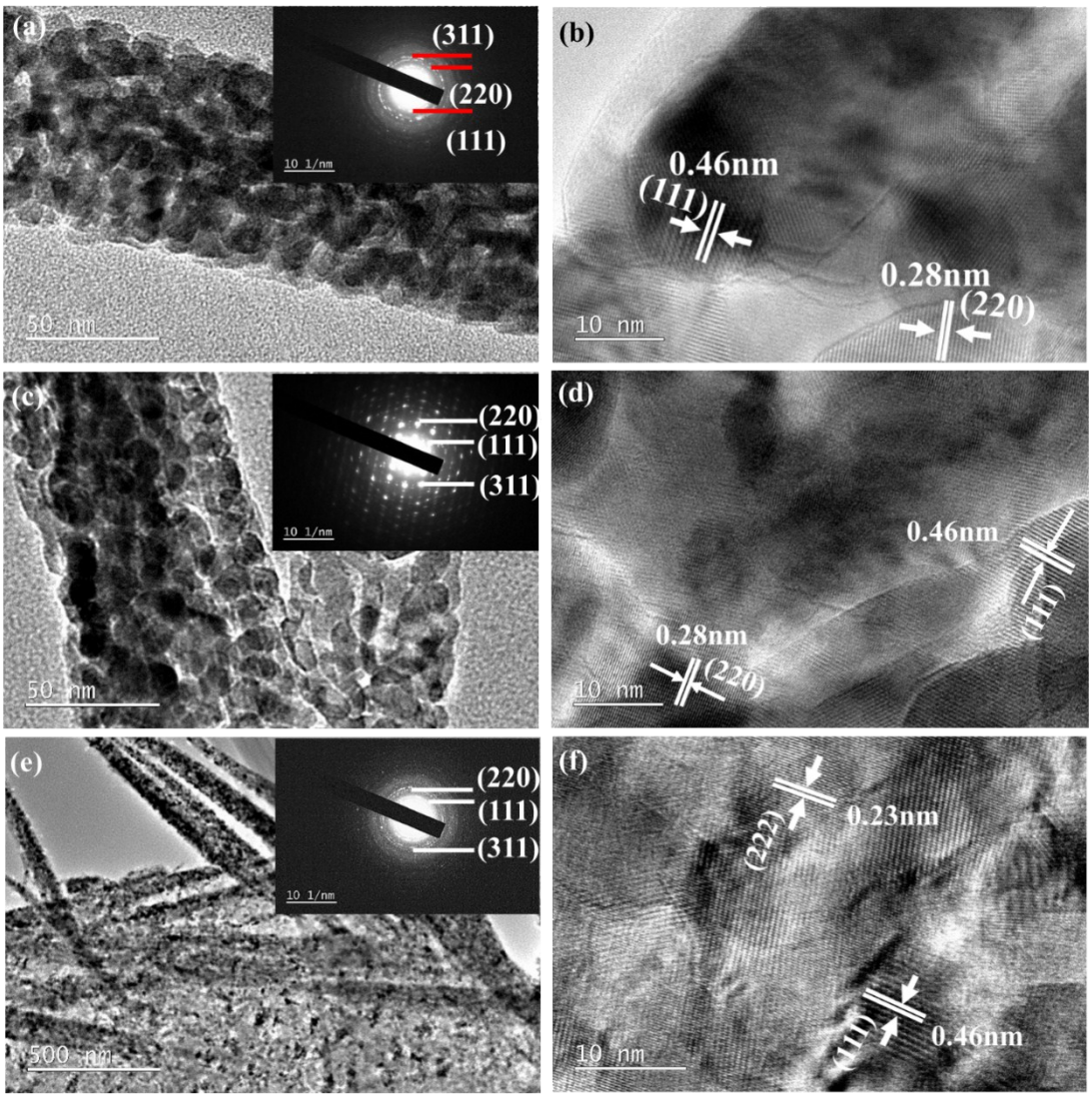

Fig. S2 (a, c, e) TEM, selected area electron diffraction (SAED)inset, and (b, d, f) HRTEM images of Co_3O_4 nanowires, nanorods and nanosheets, respectively.

The XRD pattern (Fig. S3a) reveals the crystal structure and phase purity of three types of Co_3O_4 nanoarrys. The three typical peaks were derived from Ni foam, other diffraction peaks all correspond to spine Co_3O_4 crystalline structure (PDF#43-1003). No spare impurity peaks are detected, which implied there was no impurities produced during the hydrothermal and calcination processes. The peaks at 31.27°, 36.845°, 59.35° and 65.23° correspond to (220)，(311)，(511) and (440) planes of cubic Co_3O_4 , respectively.

Nitrogen adsorption desorption isotherms of three kinds of nanoarrays are shown in the Fig. S3 b-d, they revealed the typical type-IV curve with a significant hysteresis loop at the relative pressure of 0.4-0.9. It can also be seen from the pore size distribution curve. Table S1 shows the specific surface area, pore volume and pore size of the three samples. It can be seen that the nanowire array has the largest specific surface area, and also exhibits the largest pore volume and the appropriate pore size. Compared with the other two nanoarrays, the nanowire array is more favorable for the reversible formation and decomposition of the discharge products on the surface of the nanoarrays.

Table S1 Comparison of the specific surface area, pore volume and BJH pore size of three types of Co_3O_4 nanoarrays.

Sample	Surface area（$m^2\ g^{-1}$）	Pore volume ($cm^3\ g^{-1}$)	BJH Pore size (nm)
Nanowires	16.116	4.20×10^{-2}	4.42
Nanorods	14.125	2.66×10^{-2}	4.42
Nanosheets	5.4432	2.08×10^{-2}	10.89

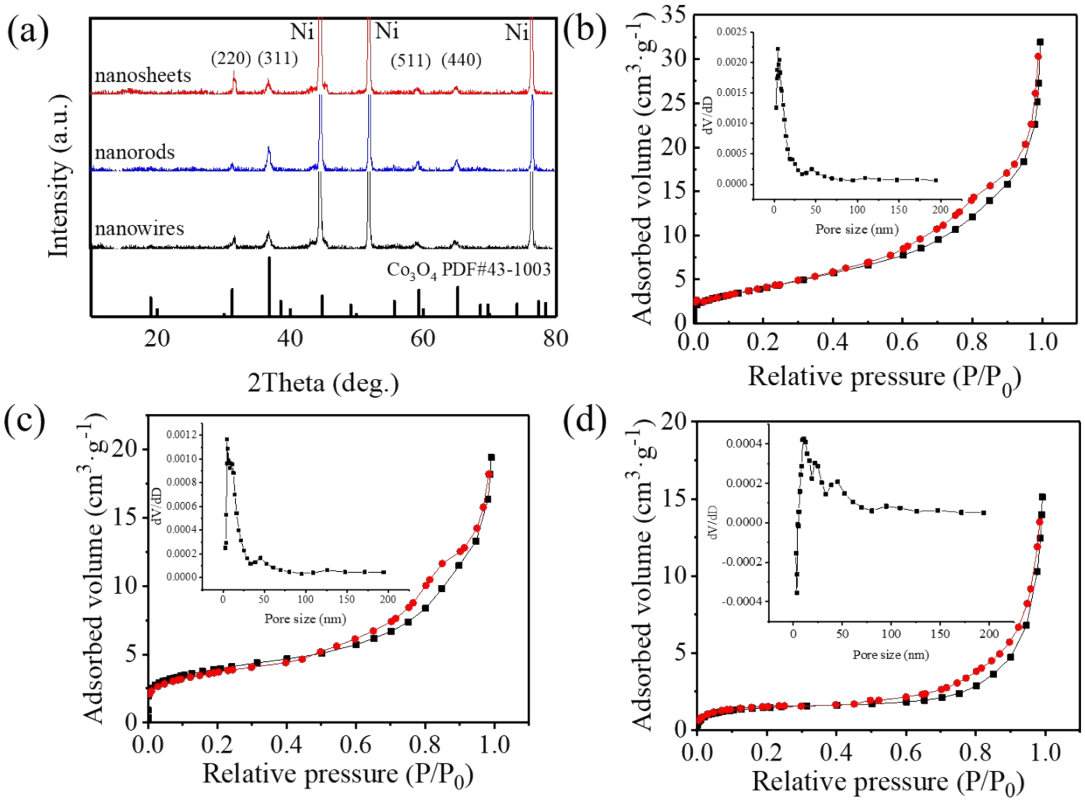

Fig. S3 (a) XRD patterns of Co_3O_4 nanoarrays. N_2 adsorption−desorption isotherms and the corresponding pore size distribution curves of Co_3O_4 (b) nanowires, (c) nanorods, and (d) nanosheets.

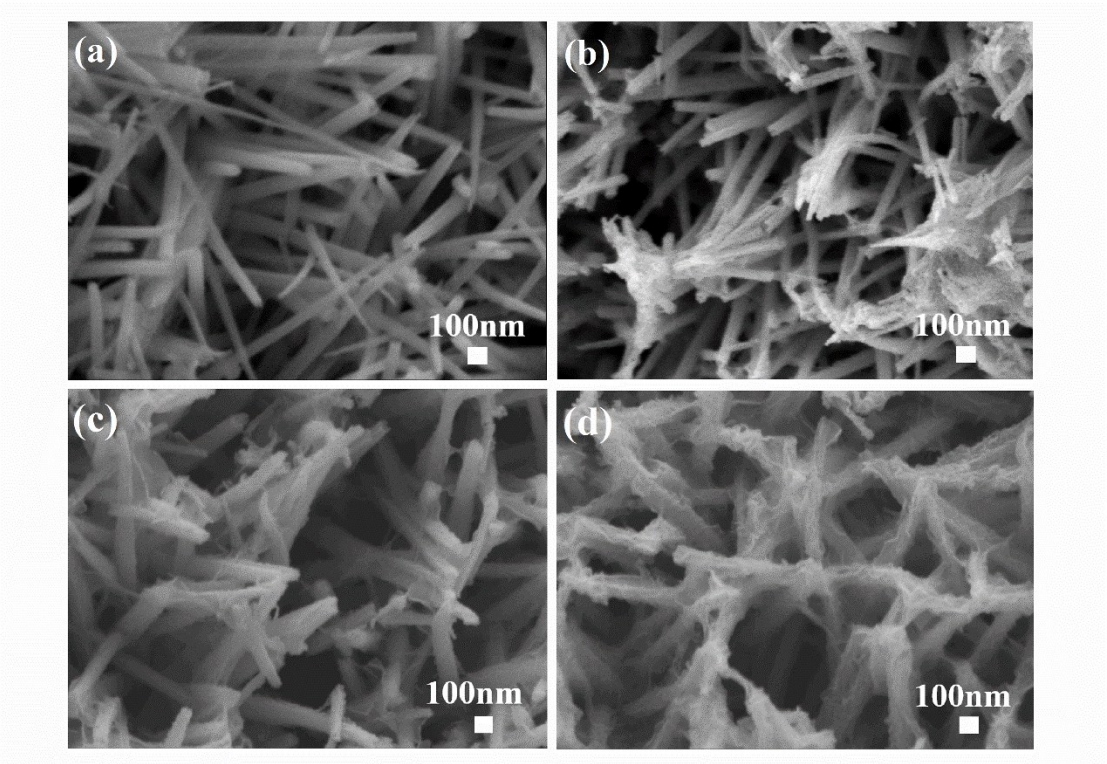

Fig.S4 FESEM images of pristine Co_3O_4@Ni(a), r-Co_3O_4@Ni-0.5(b), r-Co_3O_4@Ni-1(c) and r-Co_3O_4@Ni-2(d)

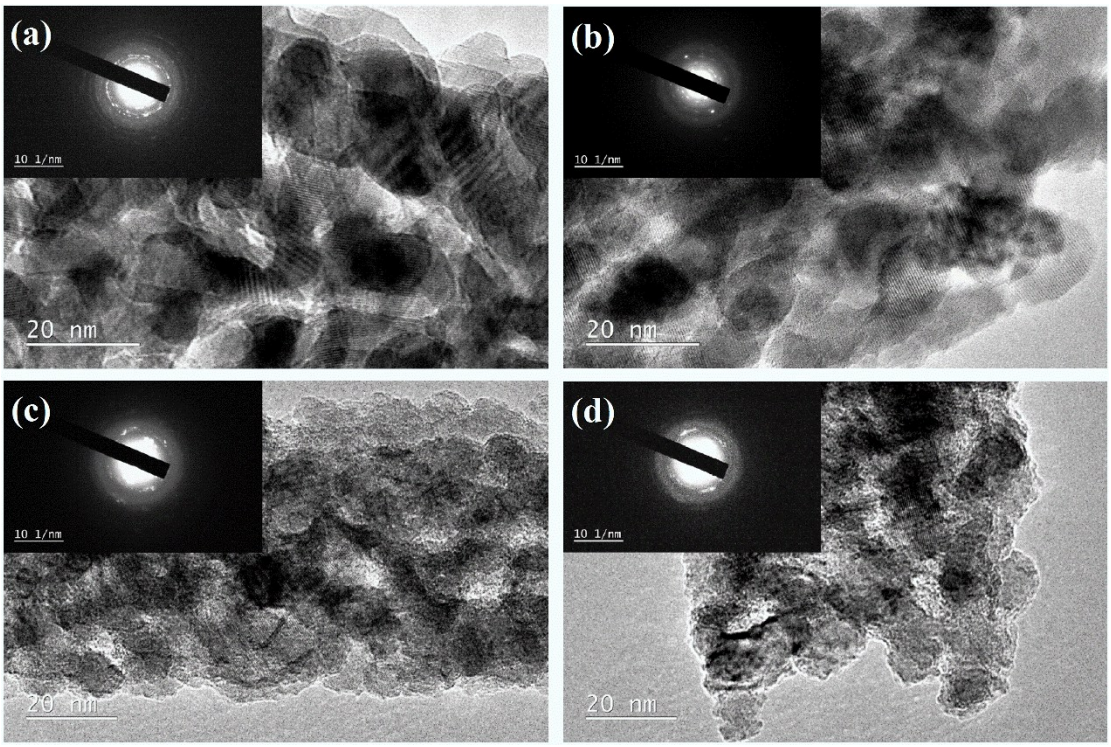

Fig. S5 The TEM images and SADE(inset) of pristine Co_3O_4(a), r-Co_3O_4-0.5(b), r-Co_3O_4-1(c) and r-Co_3O_4-2(d).

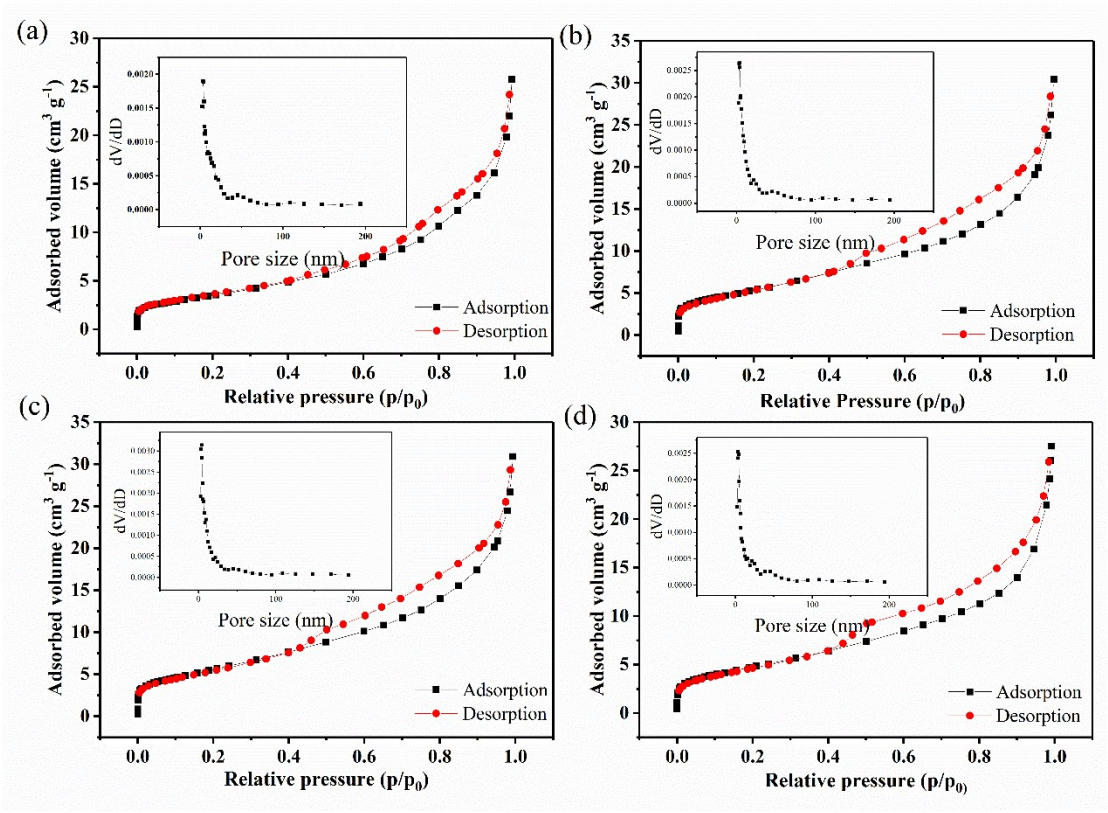

Fig. S6 N_2 adsorption−desorption isotherms and the corresponding pore size distribution curves (inset) of pristine Co_3O_4@Ni(a), r-Co_3O_4@Ni-0.5(b), r-Co_3O_4@Ni-1(c) and r-Co_3O_4@Ni-2(d).

Table S2 Comparison of the specific surface area, pore volume and BJH pore size of Co_3O_4 @Ni and reduced Co_3O_4@Ni

Sample	**BET Surface Area (m^2 g^{-1})**	**Pore Volume (cm^3 g^{-1})**	**BJH Pore size (nm)**
Co_3O_4@Ni	16.624	0.0369	3.47
r-Co_3O_4@Ni-0.5	20.344	0.041459	3.47
r-Co_3O_4@Ni-1	21.368	0.042898	3.92
r-Co_3O_4@Ni-2	17.882	0.0385	3.92

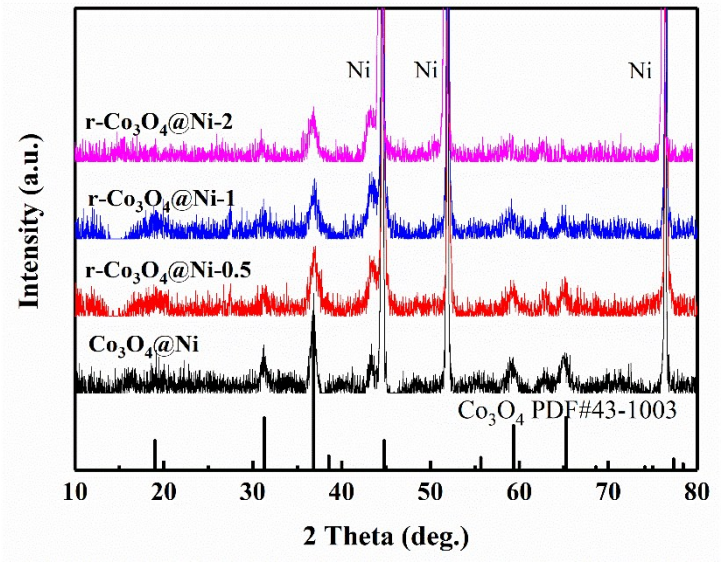

Fig. S7 XRD patterns of pristine Co_3O_4@Ni and reduced Co_3O_4@Ni

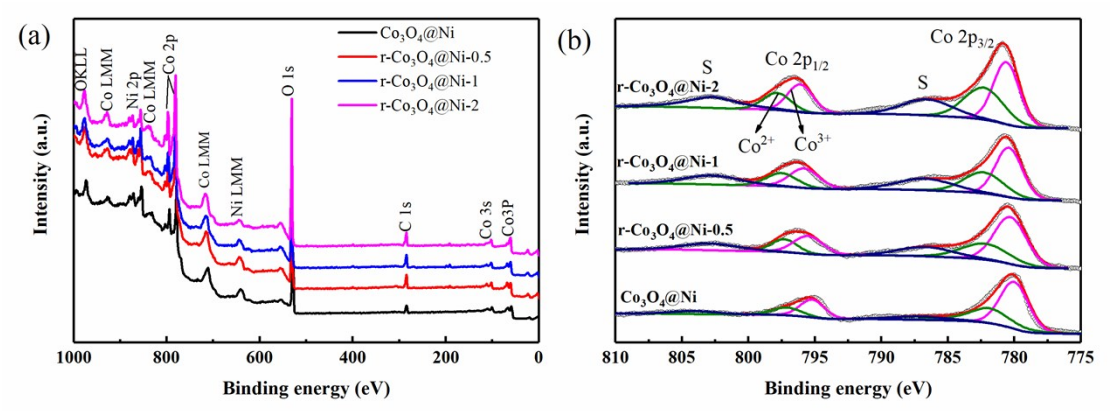

Fig. S8 (a) XPS survey spectra (b) Co 2p spectra of pristine Co_3O_4@Ni, r-Co_3O_4@Ni-0.5, r-Co_3O_4@Ni-1 and r-Co_3O_4@Ni-2.

Table S3 The molar percentage of Co^{2+} and Co^{3+} in Co_3O_4@Ni and reduced Co_3O_4@Ni

Sample	**Co^{2+} (mol%)**	**Co^{3+} (mol%)**
Co_3O_4@Ni	33.78	66.22
r-Co_3O_4@Ni-0.5	31.51	64.89
r-Co_3O_4@Ni-1	39.69	60.31
r-Co_3O_4@Ni-2	42.79	57.21

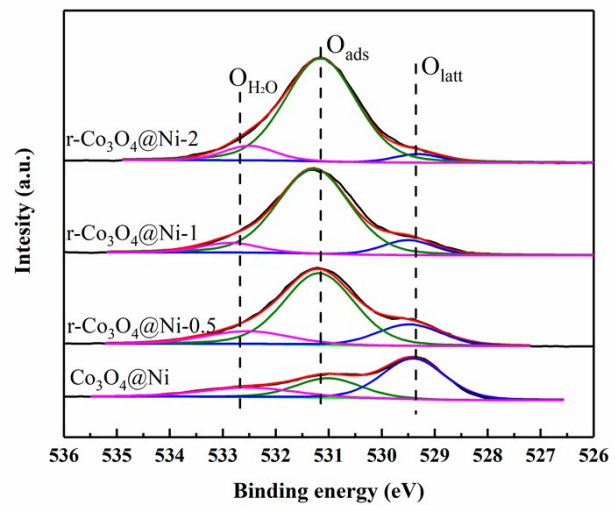

Fig. S9 O1s XPS spectra of pristine Co_3O_4@Ni and reduced Co_3O_4@Ni.

Table S4 EDS microanalysis of Co and O atomic ratio in pristine and reduced Co_3O_4@Ni electrodes.

Element / Sample	O (At%)	Co (At%)
Co_3O_4@Ni	68.91	31.09
r-Co_3O_4@Ni-0.5	63.75	36.25
r-Co_3O_4@Ni-1	62.82	37.18
r-Co_3O_4@Ni-2	53.58	46.42

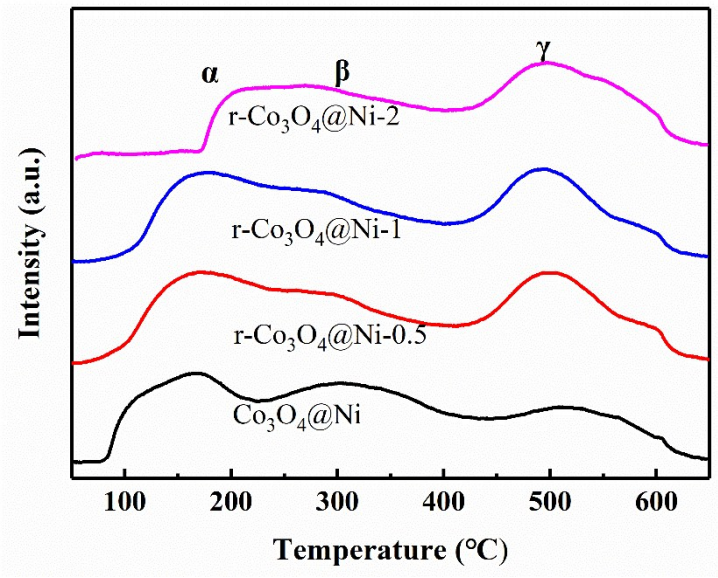

Fig. S10 O_2-TPD spectra of pristine Co_3O_4@Ni and reduced Co_3O_4@Ni.

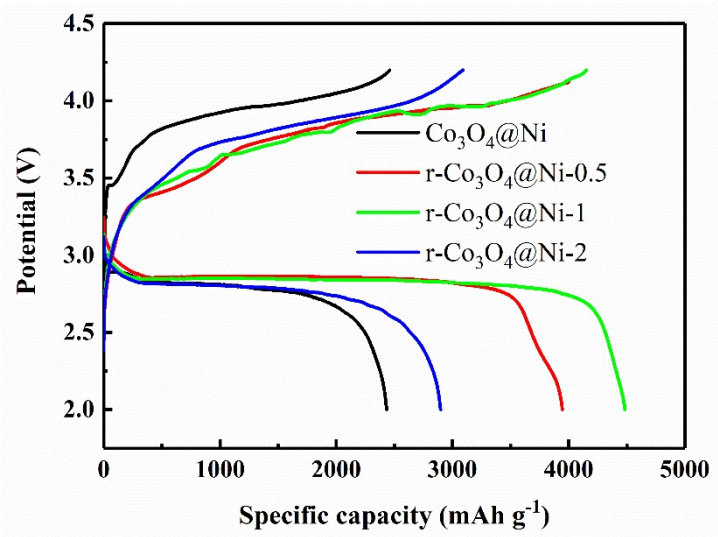

Fig. S11 Comparison of discharge/charge profiles of Li-O_2 batteries with pristine Co_3O_4@Ni and reduced Co_3O_4@Ni electrodes at 50 mA g^{-1}.

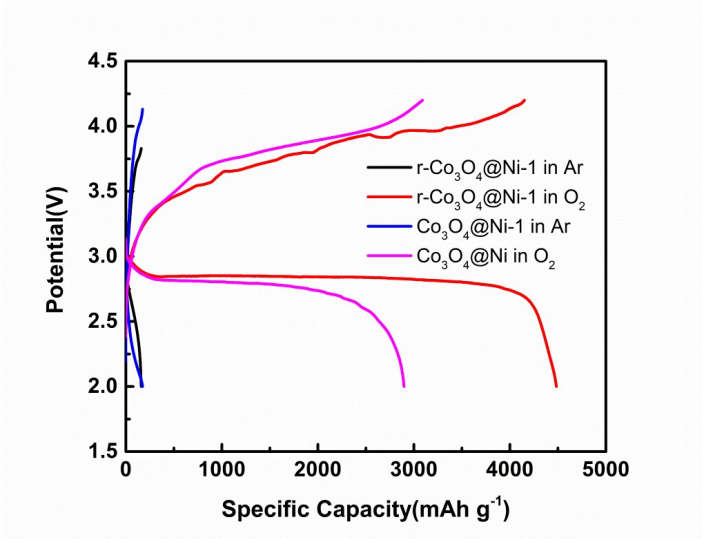

Fig.S12 Comparison of discharge/charge profiles of Li-O_2 batteries with pristine Co_3O_4@Ni and r-Co_3O_4@Ni-1 electrodes at the current density of 50 mA g^{-1} in O_2 and Ar

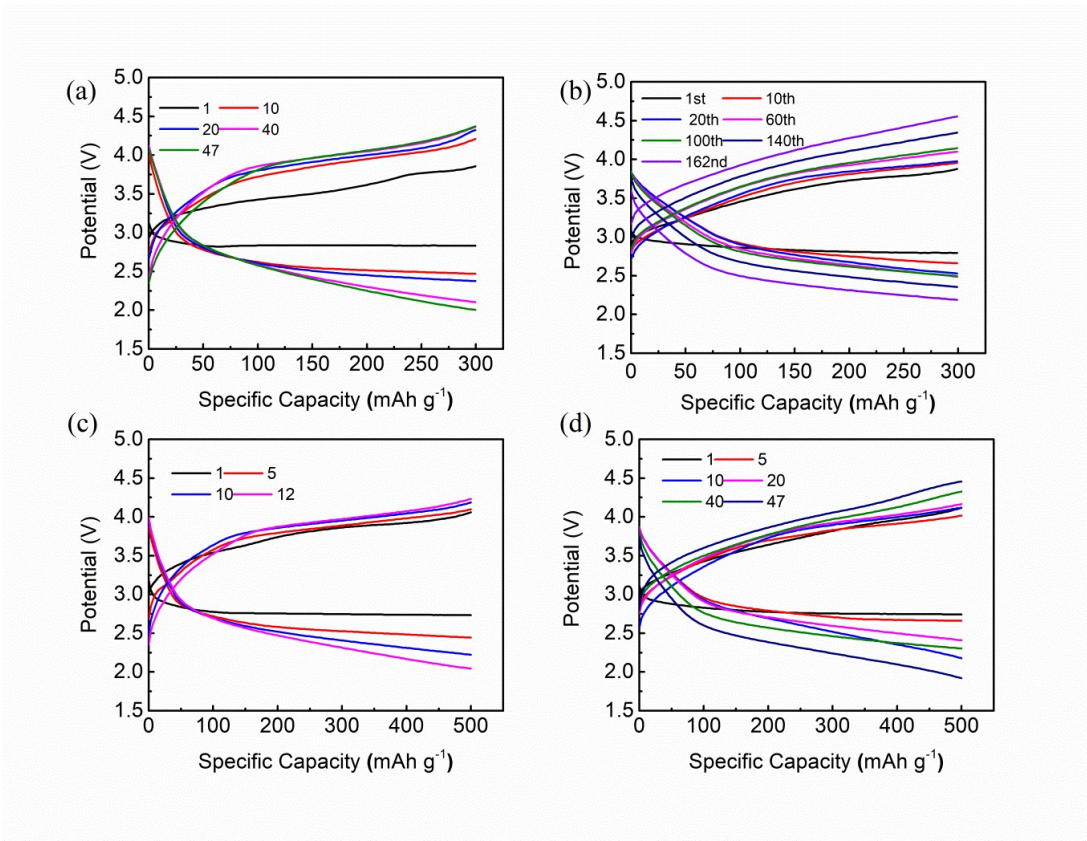

Fig.S13 Cycling performance of Li-O_2 batteries at the current density of 200 mA g^{-1} with pristine Co_3O_4@Ni (a) and r-Co_3O_4@Ni-1 (b) electrodes with the cutoff capacity of 300 mAh g^{-1}; with pristine Co_3O_4@Ni (c) and r-Co_3O_4@Ni-1 (d) electrodes with the cutoff capacity of 500 mAh g^{-1}.

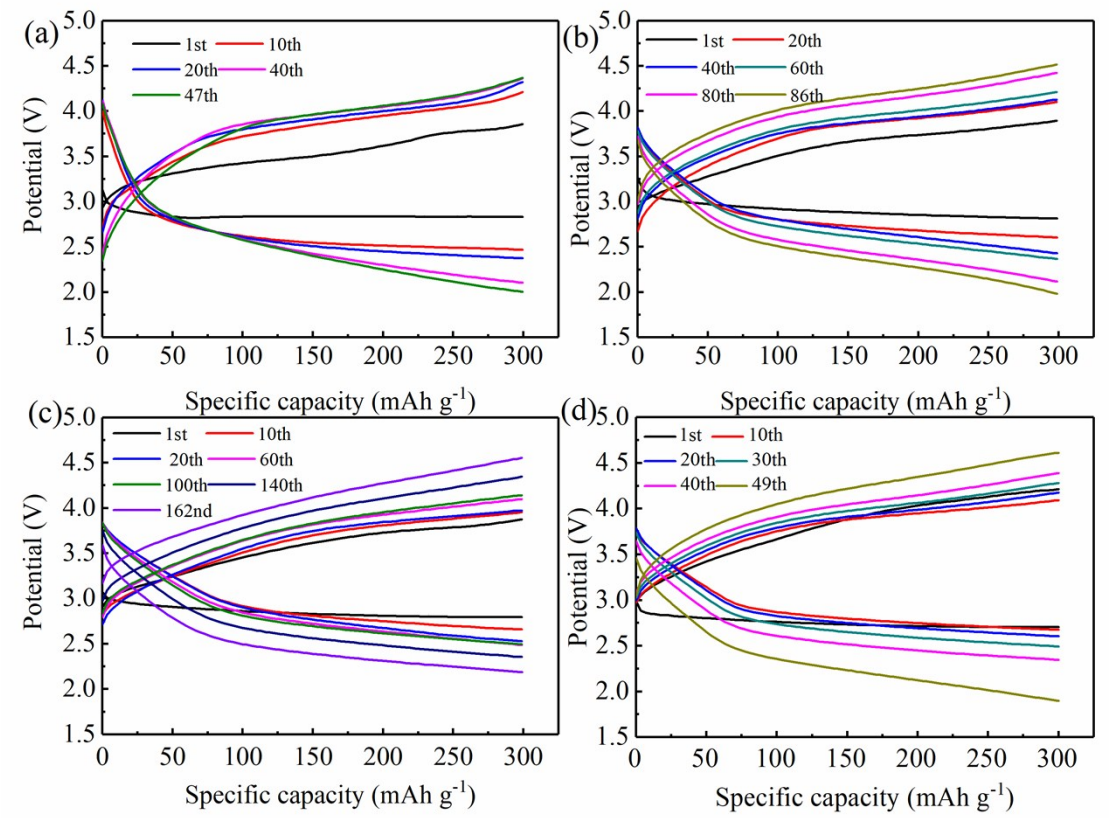

Fig. S14 Cycling performance of Li-O_2 batteries with pristine Co_3O_4@Ni(a) r-Co_3O_4@Ni-0.5(b), r-Co_3O_4@Ni-1(c) and r-Co_3O_4@Ni-2(d) electrodes at 200 mA g^{-1} with the cutoff capacity of 300 mAh g^{-1}.

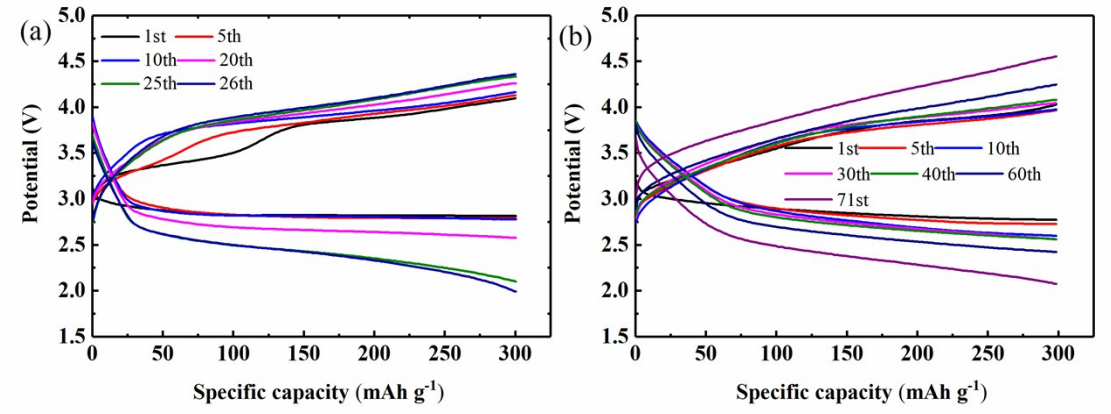

Fig. S15 Cycling performance of Li-O_2 batteries with pristine Co_3O_4@Ni(a) and r-Co_3O_4@Ni-1(b) electrodes at 100 mA g^{-1} with the cutoff capacity of 300 mAh g^{-1}.

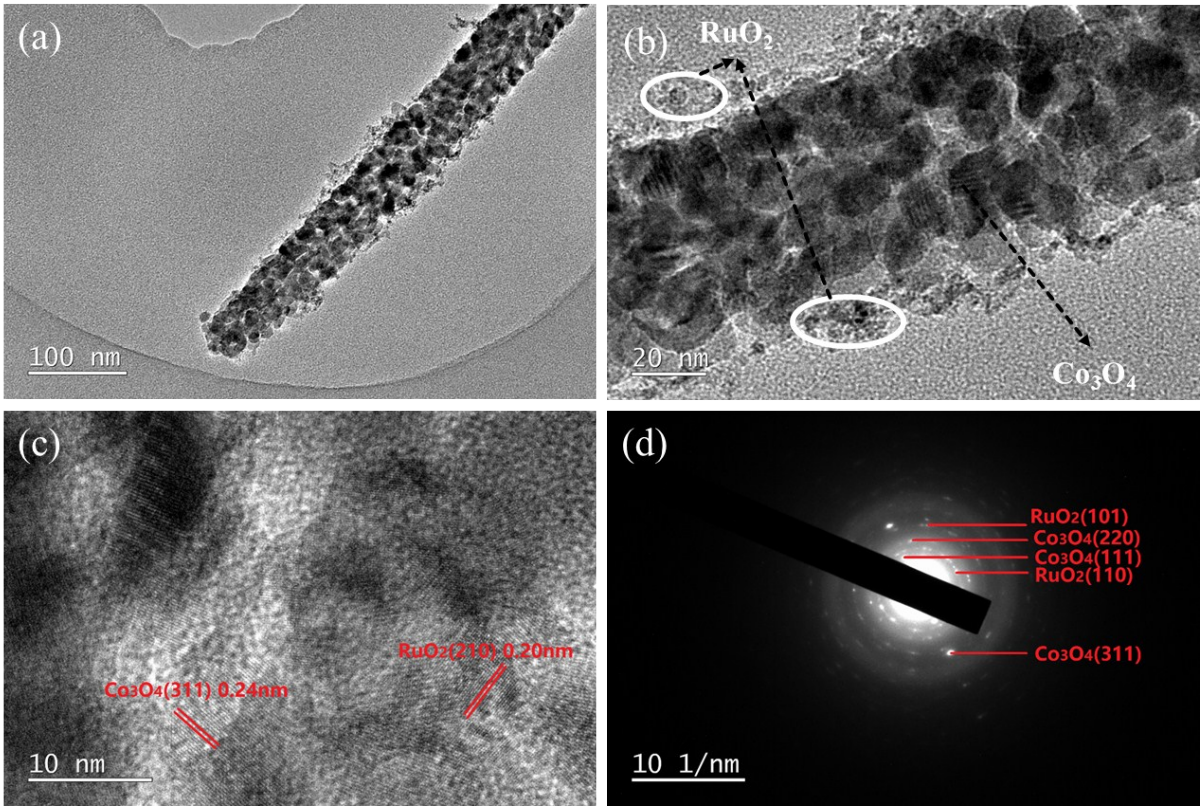

Fig. S16 TEM images of composited RuO_2/Co_3O_4 nanowires: (a, b) Low magnification TEM images; (c) HRTEM image; (d) SEAD pattern

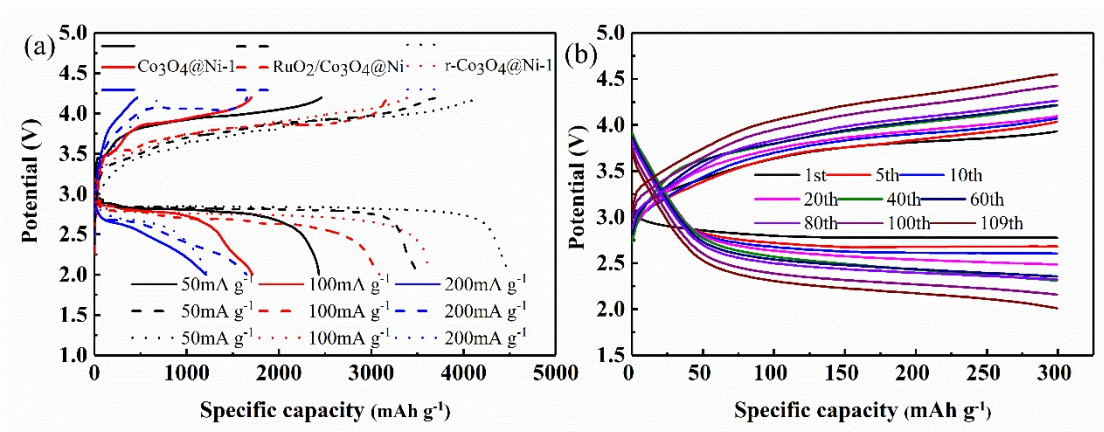

Fig. S17 (a)Comparison of discharge/charge profiles of Li-O_2 batteries with Co_3O_4@Ni, RuO_2/Co_3O_4@Ni and r-Co_3O_4@Ni-1 cathodes at various current densities of 50mA g^{-1}, 100 mA g^{-1} and 200 mA g^{-1}. (b) Cycling performance of Li-O_2 batteries with RuO_2/Co_3O_4@Ni electrode at 200 mA g^{-1} with the cutoff capacity of 300mAh g^{-1}.

Table S5 Summary of electrochemical performance of Li–O_2 batteries with RuO_2 or Ru modified catalyst.

Catalyst	Specific capacity	Cycle number	Current density	Fixed capacity	Voltage	Electrolyte	Ref
RuO_2/NiO/Ni foam	3465mAh g^{-1}, 250mA /g_{RuO2}	>200	250 mA $g^{-1}{}_{RuO2}$	500 mAh g^{-1}	2.5-4.2V	1.0 M LiTFSI/ TEGDME	[1]
RuO_2/MnO_2/Ni/G	1523 mAh g^{-1}, 3200 mA g^{-1}	170	3200 mA g^{-1}	1000 mAh g^{-1}	2.0-4.07V	1.0 M LiTFSI+0.05MLiI /TEGDME	[2]
TiO_2/RuO_2/Ti mesh	800mAh g^{-1}, 50 mA g^{-1}	>80	100 mA g^{-1}	300 mAh g^{-1}	2.3-4.5V	0.1M$LiClO_4$/ DMSO	[3]
Ru/Co_3O_4 nanosheets/carbon textiles	~9700mAh g^{-1},200 mA g^{-1}	72	200 mA g^{-1}	1000 mAh g^{-1}	2.0-4.5V	1M $LiCF_3SO_3$/ TEGDME	[4]
RuO_2/stainless steel	1000mAh g^{-1}, 100 mA g^{-1}	>100	200 mA g^{-1}	500 mAh g^{-1}	2.6-4.0V	0.5M $LiClO_4$/DMSO	[5]
RuO_2/Co_3O_4 nanowires/Ni foam	3506 mAh g^{-1}, 50 mA g^{-1}	109	200 mA g^{-1}	300 mAh g^{-1}	2.0-4.5V	1.0 M LiTFSI/ TEGDME	This work

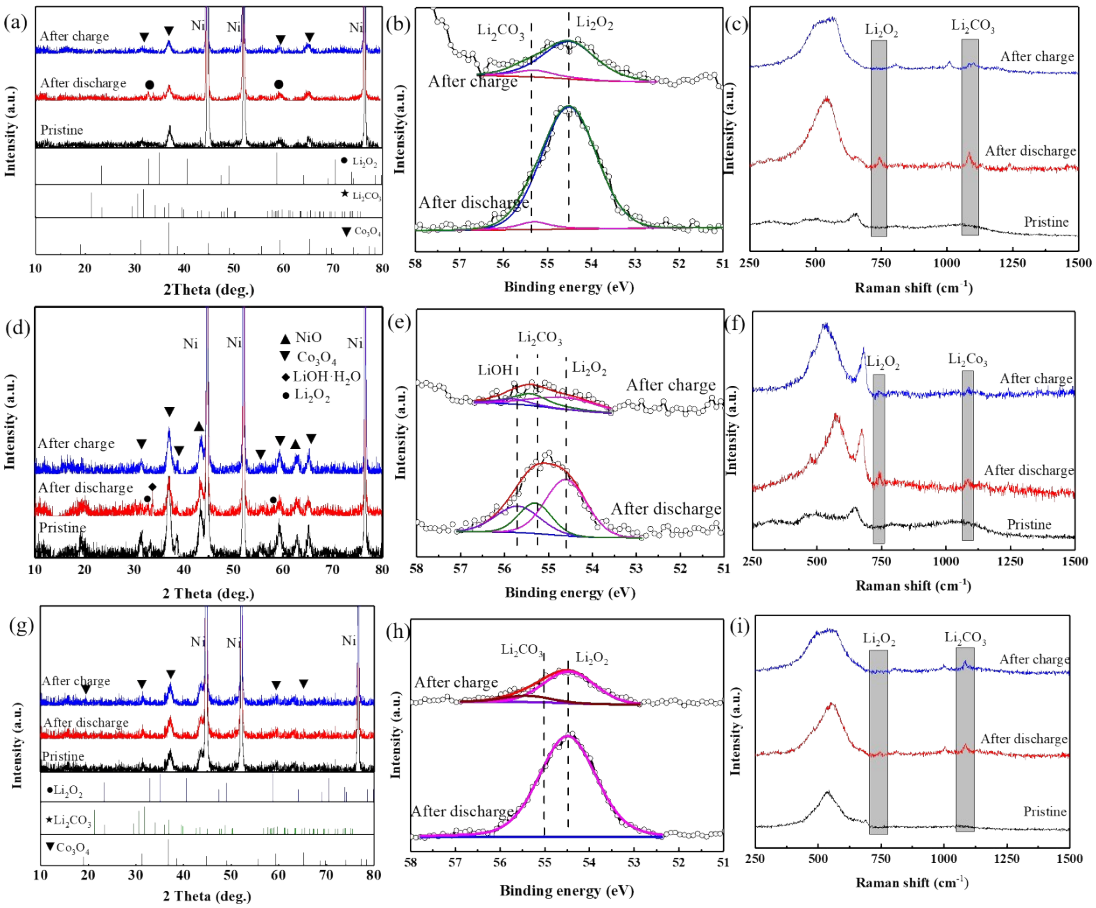

Fig. S18 XRD patterns, XPS spectra and Raman spectra of Co_3O_4@Ni(a, b, c), RuO_2/ Co_3O_4@Ni(d, e, f) and r-Co_3O_4@Ni-1(g, h, i) electrode after fully discharge and charge, respectively.

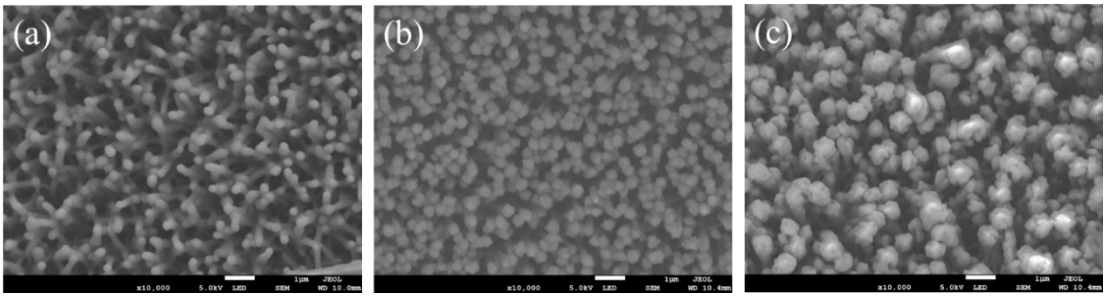

Fig. S19 SEM images of Pristine Co_3O_4@Ni electrodes after discharge to (a)500 mAh g^{-1}, (b)1000mAh g^{-1} and (c)2.0 V at the current density of 0.1 mA cm^{-2}.

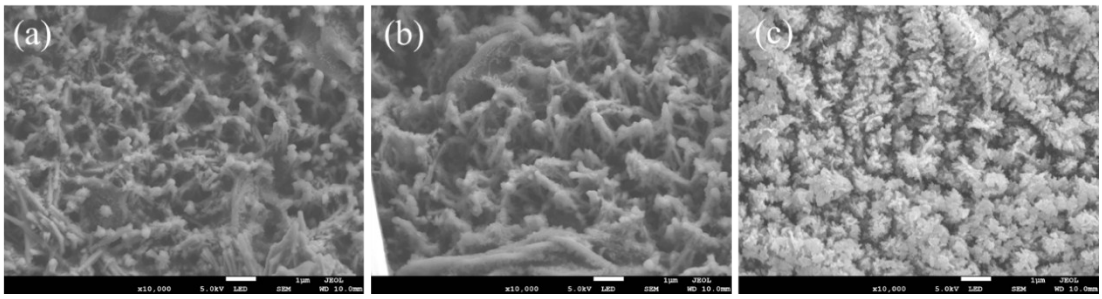

Fig. S20 SEM images of RuO_2/Co_3O_4@Ni electrodes after discharge to (a)500 mAh g^{-1}, (b)1000 mAh g^{-1} and (c)2.0 V at the current density of 0.1 mA cm^{-2}.

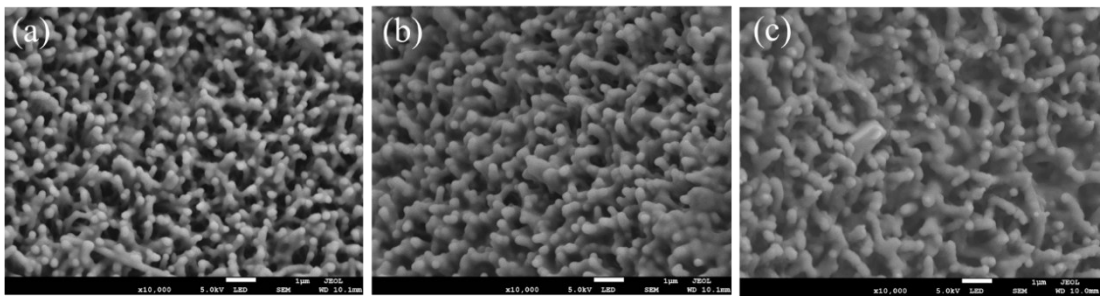

Fig. S21 SEM images of r-Co_3O_4@Ni-1 electrodes after discharge to (a)500 mAh g^{-1}, (b)1000 mAh g^{-1} and (c)2.0 V at the current density of 0.1 mA cm^{-2}.

Table S6 Summary of electrochemical performance of Li–O_2 batteries with Co_3O_4-based free-standing cathodes.

Catalyst	Specific capacity	Cycle number	Current density	Fixed capacity	Voltage	Electrolyte	Ref
Co_3O_4 nanowires/Ni foam	5337mAh g^{-1}	258 cycles with the supplement of electrolyte several times	100mA g^{-1}	500mAh g^{-1}	2.0-4.3V	1 M $LiClO_4$/ TEGDME electrolyte with Pd NCs	[6]
Reduced Co_3O_4 nanosheets/Ni foam	4565 mAh g^{-1}, 50 mA g^{-1}	90	100mA g^{-1}	500mAh g^{-1}	2.5-4.3V	0.5 M $LiClO_4$ /DMSO	[7]
Co_3O_4 nanowires/Ni foam	1380mAh g^{-1}, 50mA g^{-1}	54	100mA g^{-1}	300mAh g^{-1},	2.0-4.3V	1 M $LiCF_3SO_3$ /TEGDME	[8]
Ru/ Co_3O_4 nanowires/Ni foam	6434 mAh g^{-1}, 100 mA g^{-1}	112	100 mA g^{-1}	300mAh g^{-1}	2.0-4.3V	1M $LiClO_4$/ TEGDME	[9]
Co_3O_4 nanosheets/Ni foam	11882 mAh g^{-1} ,100 mA g^{-1}	80	200 mA g^{-1}	500mAh g^{-1}	2.0-4.5V	1 M LiTFSI/ TEGDME	[10]
Pd/ Co_3O_4 nanowires/Ni foam	1842.7mAh g^{-1}, 0.05mA/cm^2	270	0.1mA cm^{-2}	300 mAh g^{-1}	2.0-4.2V	1M $LiN(CF_3SO_2)_2$ /TEGDME	[11]
Pd/ Co_3O_4 nanosheets/Ni	1551 mAh g^{-1}, 50 mA g^{-1}	72	100 mA g^{-1}	300 mAh g^{-1}	2.0-4V	1 M LiTFSI/ TEGDME	[12]
Reduced Co_3O_4 nanowires/Ni foam	4448 mAh g^{-1}, 50 mA g^{-1}	162	200 mA g^{-1}	300 mAh g^{-1}	2.0-4.5V	1 M LiTFSI/ TEGDME	This work

To investigate the valence change of Co element, XPS test was conducted on the r-Co_3O_4@Ni-1 electrode after 5 cycles (Fig. S22) and 50 cycles (Fig. S23). The Co 2p spectra can be also deconvoluted into the characteristic peaks of Co^{2+} and Co^{3+}. The molar percentages of Co^{2+} and Co^{3+} before and after 5, 50 cycles are presented in Table S7. The percentage of Co^{3+} slightly increase after 5 and 50 cycles, indicating the oxidation of r-Co_3O_4@Ni-1 material during the discharge/charge process. The gradual oxidation of electrode material is also one of the reasons for the increasing overpotential during the cycle test[13].

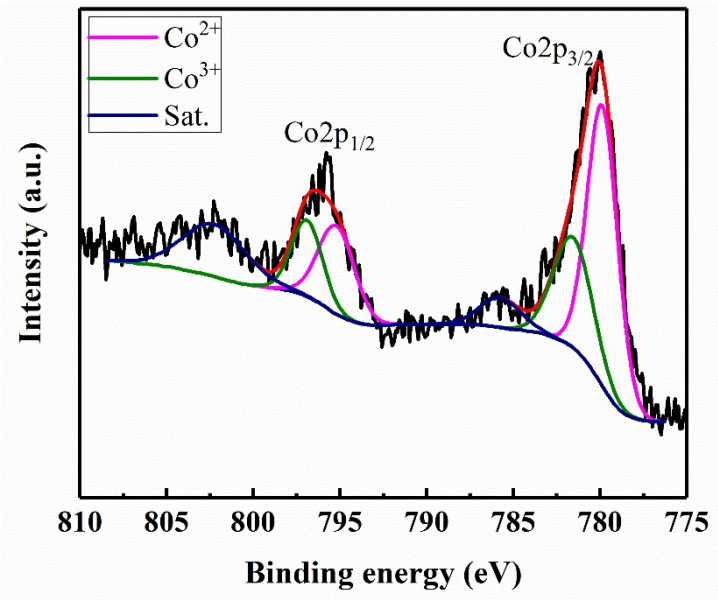

Fig. S22 Co 2p XPS of r-Co_3O_4@Ni-1 electrode after 5th cycle.

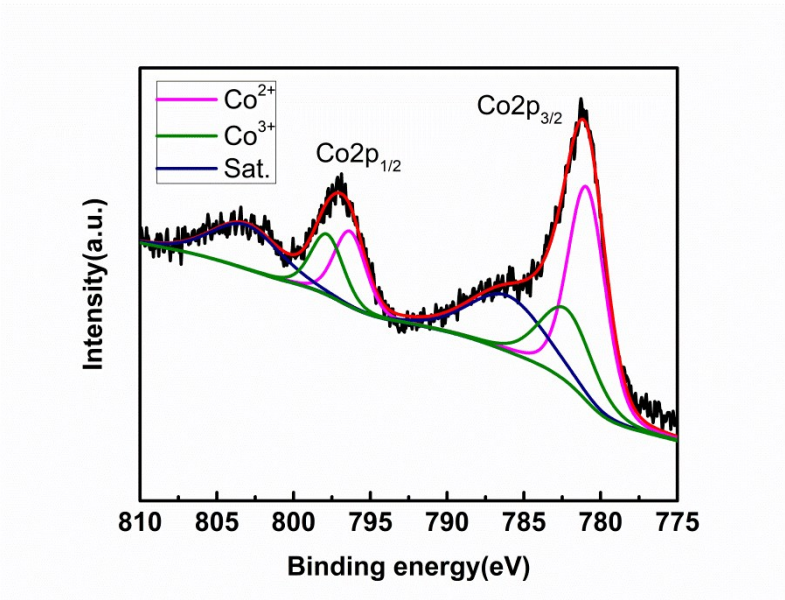

Fig. S23 Co 2p XPS of r-Co_3O_4@Ni-1 electrode after 50th cycle.

Table S7 The molar percentage of Co^{2+} and Co^{3+} in r-Co_3O_4@Ni-1 before and after 5th, 50th cycle

Sample	Co^{2+} (mol%)	Co^{3+} (mol%)
r-Co_3O_4@Ni-1	39.69	60.31
5th charged r-Co_3O_4@Ni-1	36.21	63.79
50th charged r-Co_3O_4@Ni-1	35.75	64.25

The EIS spectrums of Li-O_2 batteries with the pristine and reduced Co_3O_4@Ni cathode are shown in Fig. S24, respectively. The spectra all consist of an arc in the high frequency region and a straight line in low frequency region. Similar internal resistances of the batteries can be observed for the similar internal structure of the cathodes. While the interface impedance and charge transfer impedance increased after $NaBH_4$ treatment, which may result from the slightly surface effect on 3D network structure during reduction treatment.

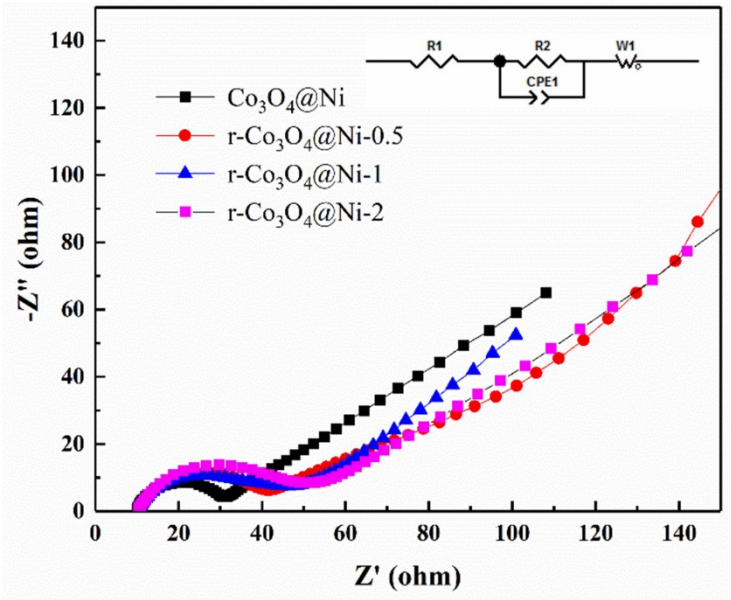

Fig. S24 EIS spectrums of three kinds of Li-O_2 batteries with the pristine and reduced Co_3O_4@Ni cathode.

Table S8 Electrolyte resistance (R_s),interfacial resistance(R_{int}),calculated from impedance plots by fitting using the equivalent circuit

Sample	**R_s(Ω)**	**R_{int}（Ω）**
Co_3O_4@Ni	9.002	16.3
r-Co_3O_4@Ni-0.5	9.777	27.02
r-Co_3O_4@Ni-1	10.01	33
r-Co_3O_4@Ni-2	9.654	32.41

[1] P. Tan, Z.H. Wei, W. Shyy, T.S. Zhao, X.B. Zhu, Energy Environ. Sci. 9 (2016) 1783-1793.

[2] G. Wang, L. Huang, W. Huang, J. Xie, G. Du, S. Zhang, P. Zhu, G. Cao, X. Zhao, Nanoscale 7 (2015) 20614-20624.

[3] Z. Guo, C. Li, J. Liu, X. Su, Y. Wang, Y. Xia, J. Mater. Chem. A 3 (2015) 21123-21132.

[4] Q.-c. Liu, J.-j. Xu, Z.-w. Chang, D. Xu, Y.-b. Yin, X.-y. Yang, T. Liu, Y.-s. Jiang, J.-m. Yan, X.-b. Zhang, Part. Part. Syst. Char. 33 (2016) 500-505.

[5] C. Zhang, D. Tang, X. Hu, X. Liu, T. Zhang, H. Zhou, Energy Stor. Mater. 2 (2016) 8-13.

[6] C. Cao, Y. Yan, H. Zhang, J. Xie, S. Zhang, B. Pan, G. Cao, X. Zhao, ACS Appl. Mater. Inter. (2016).

[7] C. Shen, Z. Wen, F. Wang, X. Huang, K. Rui, X. Wu, RSC Adv. 6 (2016) 16263-16267.

[8] M. He, P. Zhang, S. Xu, X. Yan, ACS Appl. Mater. Inter. 8 (2016) 23713-23720.

[9] L. Huang, Y. Mao, G. Wang, X. Xia, J. Xie, S. Zhang, G. Du, G. Cao, X. Zhao, New J. Chem. 40 (2016) 6812-6818.

[10] F. Wu, X. Zhang, T. Zhao, R. Chen, Y. Ye, M. Xie, L. Li, J. Mater. Chem. A 3 (2015) 17620-17626.

[11] L. Leng, X. Zeng, H. Song, T. Shu, H. Wang, S. Liao, J. Mater. Chem. A 3 (2015) 15626-15632.

[12] R. Black, B. Adams, L.F. Nazar, Adv. Funct. Mater. 2 (2012) 801-815.

[13] C. Shen, Z. Wen, F. Wang, T. Wu, X. Wu, ACS Catal. 6 (2016) 4149-4153.